Proceedings of GPPS Forum 18
Global Power and Propulsion Society
Montreal, 7th-9th May 2018
www.gpps.global

GPPS-2018-0052

EXPERIMENTAL INVESTIGATION OF AN SOFC OFF-GAS COMBUSTOR FOR HYBRID POWER PLANT USAGE WITH LOW HEATING VALUES REALISED BY NATURAL GAS ADDITION

Timo Lingstädt, Felix Grimm, Thomas Krummrein, Sandro Bücheler, Manfred Aigner
German Aerospace Center (DLR)
timo.lingstaedt@dlr.de
Stuttgart, Germany

ABSTRACT

Rising power demands and the increasing importance of decentralised energy production based on renewable resources require gas turbine systems with flexible energy conversion.

Therefore, a suitable hybrid power plant demonstrator with a high temperature fuel cell is being set up at the German Aerospace Centre (DLR). This facility requires burner concepts for low calorific gases capable of combusting the exhaust products of the fuel cell system anode side, here referred to as SOFC (solid oxide fuel cell) off-gas. The combustor behaviour for the demonstrator system is investigated in the current work using an atmospheric combustor test rig at DLR. Additionally, a strategy for stabilisation of the flame in operating points with very low heating values (LHV) via addition of natural gas into the SOFC off-gas before entering the combustor is tested in view of expected impacts on efficiency and other critical system parameters. The combustion system is furthermore investigated in view of CO emissions.

INTRODUCTION

Conventional fossil fuels are a highly demanded but at the same time limited energy source. As a matter of fact, global electrical energy needs to increase rapidly. Thus, it is important to develop power plant concepts with high efficiency. One promising concept is the SOFC/MGT (micro gas turbine) hybrid power plant, as currently being developed and built as a demonstrator at German Aerospace Center (DLR) in a collaboration of the Institute of Combustion Technology (VT) and the Institute of Engineering Thermodynamics (TT) (Hohloch et al., 2017). Hybrid power plants not only provide a large potential for efficiency increase but also for emissions reduction and operational flexibility. The presented work is based on a system, which integrates a solid oxide fuel cell emulator into a standard micro gas turbine cycle between compressor and turbine, as shown in Fig. 1. The generator "G" is mounted on the shaft

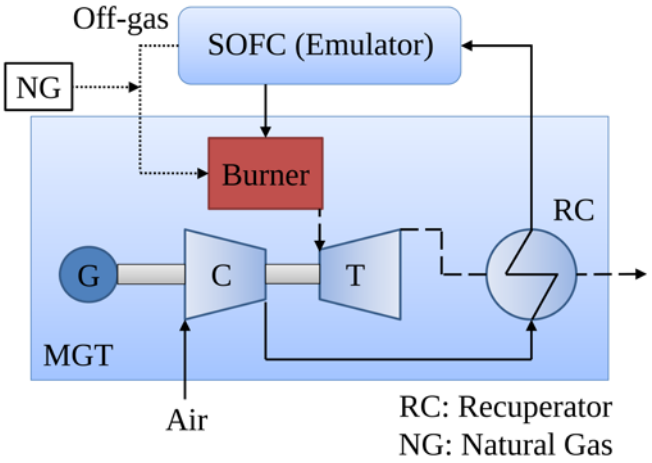

Figure 1 Hybrid Power Plant Cycle with Off-Gas Emulation Concept.

conventionally and the original recuperator from the micro gas turbine system, providing the necessary operating temperatures for the SOFC, is located prior to the SOFC (Emulator). The anode-side exhaust from the fuel-cell (referred to as SOFC-offgas) is used as fuel in the combustion chamber, while the cathode-side exhaust is used as oxidiser. The offgas typically consists of about 0.5 – 2 % H_2, 5 – 10 % CO, around 40 % H_2O and 50 % CO_2. This leads to an LHV around 1 - 3 MJ/kg, depending on the operating point and initial fuel. Since the fuel-cell uses a significant amount of the contained oxygen, the oxidiser is characterised by a reduced O2-content compared to air of about 15 - 18 %.

For the presented work, an atmospheric test rig is used in order to characterise the developed burner towards its final

purpose of running in the power plant under very low-caloric, hybrid conditions. Those are provided as operational boundary conditions from the overall power plant specifications via numerical cycle simulations. The investigated burner is coupled with an SOFC emulator (Bücheler et al., 2017) in order to simulate the thermodynamic and fluid dynamic properties of an actual fuel cell. An additional natural gas supply is used for stability reasons in part load operation with the low caloric off-gas.

As mentioned previously, one of the key features of the power plant demonstrator is operational flexibility. Therefore, the developed burner has to provide a wide operational range, including SOFC off-gas and standard micro gas turbine operation. As pointed out by (Bücheler et al., 2017), existing SOFC applications employ catalytic or conventional diffusion combustion systems (Hermann et al., 2002; Loukou et al., 2009; Voss et al., 2009), which are not particularly suited for attached turbine processes. In the present work, a partially premixed, jet-stabilised FLOX®-similar combustor is used.

The FLOX® concept was originally designed as volumetric or MILD combustion for the use in industrial furnaces (Wünning et al., 1997; Cavaliere et al., 2004). In the latest MGT combustion systems however, the jet-stabilised combustion features mainly discrete flames rather than volumetric combustion, which is only achieved under very lean part load conditions. Fuel is injected coaxially in the main flow direction in order to partially premix air and fuel in an upstream mixing section before entering the combustion chamber. Due to the rather high jet velocities, a strong inner recirculation zone is present, where hot gases consisting of combustion products are transported back to the reaction zone. The results are a relatively homogeneous temperature distribution, a wide and stable operating range, and low emissions (Flamme 2001; Lückerath et al. 2008). Furthermore, the flame flashback risk is reduced due to the high jet velocities, even for fuel with large flame speeds such as hydrogen (Flamme 2004; Lammel et al., 2011). As summarised by (Bücheler et al., 2017), such jet-flame based FLOX® systems were extended with swirl-stabilised pilot stage burners, in order to further extend the burner operating range (Rödiger et al., 2013; Zanger et al., 2013; Monz et al., 2015).

The combustor investigated in this work is based on a twelve nozzle jet-stabilised concept (Bücheler et al., 2017) designed with regard to low total pressure loss while still providing high flexibility and stability. It is depicted in Fig. 2. The test rig consists of a controlled electrical air heating device providing the relatively high combustor inlet temperatures for the hybrid power plant application. Additionally the possibility to add N_2 to the air is given, taking into account the reduced O_2-content of the fuel cell cathode exhaust used as "air" in this case. The O_2-content can be controlled by mixing the appropriate amount of N_2 to the airflow, while keeping the total flow of the mixture constant. A so called superheated steam generator, a device specifically developed to provide the required gas composition modelling the SOFC off-gas at a high temperature level, is connected as fuel supply to the test rig. This component is based on a hydrogen combustion chamber running under fuel-rich conditions equipped with the possibility to mix in the appropriate amounts of CO and CO_2. The test rig is optically accessible. The integrated OH*-chemiluminescence signal and exhaust gas analysis are used for evaluation of the burner behaviour.

Since an important adjustment to the system design for the demonstrator has been made, the operating conditions for the combustion chamber have changed significantly since the last investigations carried out in (Bücheler et al., 2017). A remarkable decrease of the resulting LHVs in the off-gas over the complete operational range of the power plant has demanded new investigations especially of the critical part load case and has led to new challenges guaranteeing a stable combustion over the whole operational range. These issues are addressed in the presented work.

BURNER SETUP

The examined burner is shown in Fig. 2. It is tested on an atmospheric test rig with optical access through quartz glass windows.

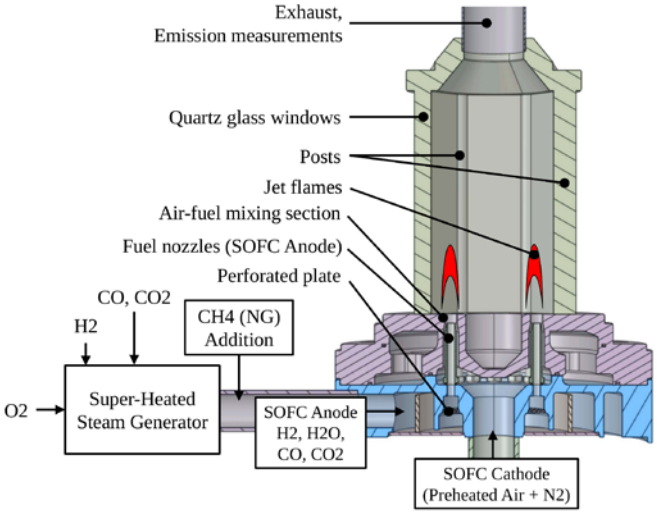

Figure 2 Sketch of the burner and the upstream steam generator setup.

As introduced previously, the SOFC is not explicitly used for atmospheric tests, but is substituted by an upstream superheated steam generator which is essentially a H_2/O_2 burner that realises the necessary anode temperatures and compositions, as they would be produced by a fuel cell. This steam generator is designed to be able to realise a large range of operating conditions, as given by the overall hybrid power plant operational range. The steam generator is divided into a combustion chamber with rich H_2/O_2 conditions to provide the necessary H_2 and H_2O content in the exhaust gas and a downstream section, where CO and CO_2 are injected. Natural gas can be added to the steam generator exhaust gas. This is done to provide stable combustion in case of part load conditions, which is challenging in this particular application due to very low LHV and resulting low adiabatic flame temperatures.

The off-gas is then redirected and led through a perforated plate, before it enters the combustion chamber through twelve annularly arranged fuel nozzles. The oxidiser is represented by a preheated mixture of air and added N_2 that is injected centrally and distributed equally by an upstream plenum to reach the premixing zone around the twelve fuel nozzles in order to realise a partially premixed regime in co-flow alignment.

After a short premixing zone, the partially premixed gas issues into the combustion chamber, where discrete jet flames form the reaction zone. Combustion products then leave the combustion chamber through an exhaust duct, where exhaust gas measurements are carried out.

SOFC Burner Operating Range

For investigation of the combustor behaviour in the context of the hybrid power plant system before implementing it into the demonstrator system, two main operating points were selected. One base load point with a high electrical system power output (labeled #1b in Fig. 3) and one part load point with a moderate electrical system power output (labeled #1p in Fig. 3). All further investigations are based on these two reference points.

The expected operating characteristic for constant stack temperatures of the fuel cell of both 1073 K (dotted line) and 1123 K (solid line) are depicted in Fig. 3. The higher temperature operating level is characterised by a higher overall electrical efficiency

$$\eta_{el} = \frac{P_{el\_SOFC} + P_{el\_Generator}}{\dot{m}_{fuel} * LHV_{fuel}} \quad (1)$$

of the system, since the fuel utilisation of the fuel cell is higher. These two temperature levels represent the thermal operational boundaries of the fuel cell system, hence the area between them can be considered as the possible steady state operational range of the power plant system. Two rotational

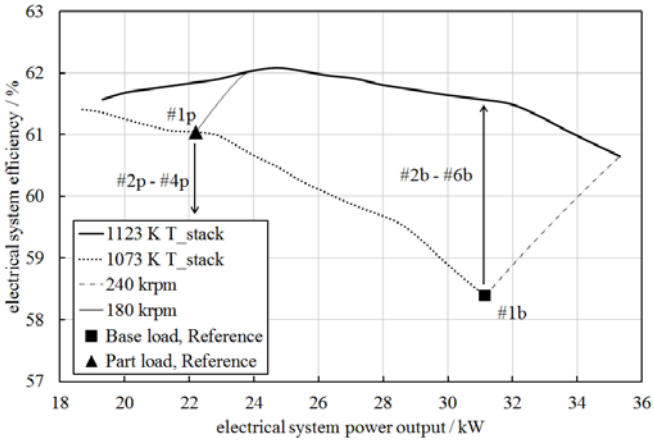

Figure 3 Base load and part load operating points – system efficiency over power output.

speed characteristics are added to the graph to visualise the operating range in terms of turbine shaft speed, higher rpm obviously located at higher system power outputs.

The addition of natural gas directly prior to the combustion chamber shifts the part load point to lower overall system efficiences while improving the operational stability conditions for the combustor and thus should be considered only when unavoidable due to unstable operation. The investigations addressing this topic are carried out in the present paper and are labelled with #2p - #4p in Fig. 3.

The increase of the fuel cell stack temperature under base load conditions on the other hand is shifting the operating point to higher system efficiencies, hence recommended for operation whenever possible. The operating point is shifting in the efficiency plot as illustrated with the arrow labeled #2b - #6b in Fig. 3. The higher fuel utilisation in the SOFC leads to a lower remaining LHV in the off-gas. The limits for this stack temperature increase due to degrading operating conditions for the combustor are pointed out in this work.

Investigated Operating Conditions

The burner is investigated for operation at base and part load conditions. The carried out studies also include a natural gas addition to the steam generator exhaust gas (anode fuel side for the burner) and a variation of fuel cell stack temperature at base load conditions. The stack temperature is the process temperature of the fuel cell. Higher stack temperatures are resulting in higher system (power plant) efficiency but on the other hand mean more critical operating conditions for the burner, since lower heating values are realised and the compositions for hydrogen and carbon monoxide on the anode side are different. Anode and cathode off-gas properties as well as the corresponding parametric studies properties are listed in Tables 1 and 2.

Table 1 Base load conditions for anode and cathode off-gas. #1b: Reference case base load, #2b - #6b: Stack temperature variations.

Anode off-gas compositions:

Case	*T [K]*	*p [kPa]*	*H2 [%]*	*CO [%]*	*H2O [%]*	*CO2 [%]*
#1b	1051	294.4	1.48	9.67	39.57	49.28
#2b	1060	278.8	1.26	8.47	40.42	49.85
#3b	1070	267.9	1.10	7.58	41.06	50.25
#4b	1079	259.7	0.96	6.82	41.61	50.61
#5b	1089	254.4	0.84	6.14	42.08	50.94
#6b	1099	250.4	0.74	5.54	42.48	51.25

Cathode off-gas compositions:

Case	*#1b*	*#2b*	*#3b*	*#4b*	*#5b*	*#6b*
O2 [%]	17.12	16.72	16.38	16.07	15.81	15.59
N2 [%]	82.88	83.28	83.62	83.93	84.19	84.41

The inlet condition values from Tables 1 and 2 were obtained from 0D thermodynamic cycle simulations according to the hybrid power plant specifications. Temperatures and pressures of the cathode off-gas side are not explicitly listed in Table 1, since they do not significantly

differ from anode values. The gas compositions of the cathode side in the part load cases are constant at 15.73 % and 84.27 % for oxygen and nitrogen, respectively.

Realised lower heating values in the experiments are depicted in Fig. 4. Remarkable are the extremely low heating values in the range of 1 to 3 MJ/kg compared to e.g. natural gas, with a lower heating value of around 49 MJ/kg. From that it becomes evident that certain operating points, especially in part load mode, cannot be run with stable combustion unless there is some kind of stabilisation involved. Therefore, for the part load cases, natural gas is added to the anode off-gas after the steam generator. The corresponding added power amounts to 1, 2 and 5 kW for the cases 2p, 3p and 4p, respectively.

The stack temperature of the fuel cell in base load operation is 1073 K. Each variation of stack temperature and an according variation of gas composition in Table 1 (cases

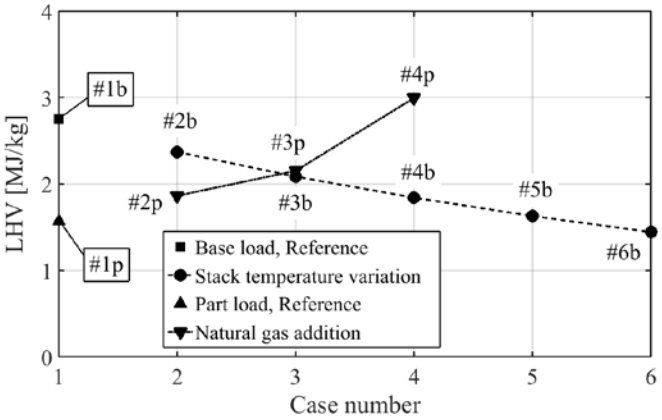

Figure 4 Depiction of lower heating values (LHV) for the experimentally investigated operating conditions.

2b – 6b) denotes a temperature increment of 10 K up to 1123 K, as reflected by inlet temperature values on the anode side as listed in Table 1. The difference between the stack temperatures and the inlet temperatures in Table 1 is a result of the heat loss taken into account by the system simulations. For all atmospheric investigations, the mass flows have been pressure corrected from the according pressure level to ambient conditions at test rig altitude to guarantee appropriate flow states in the non-pressurised test rig. Since the pressure ratio of the system is relatively low with about 3 at maximum shaft speed, the assumption of ideal gas is evaluated to be adequate for the correction. Hence the mass flows have been corrected with the ratio between actual ambient pressure at test rig location and respective operating point nominal pressure.

Table 2 Part load conditions for anode off-gas and anode natural gas addition. #1p: Reference case part load, #2p - #4p: Natural gas addition.

Anode off-gas compositions:

Case	T [K]	p [kPa]	H2 [%]	CO [%]	H2O [%]	CO2 [%]
#1p	1041	194.4	0.85	5.50	41.89	51.76
#2p	1041	194.4	0.846	5.46	41.63	51.43
#3p	1041	194.4	0.841	5.42	41.36	51.10
#4p	1041	194.4	0.825	5.32	40.58	50.14

Natural gas addition (anode off-gas side):

Case	#1p	#2p	#3p	#4p
NG [%]	0.00	0.641	1.279	3.135
Δ [***kW***]	0	1	2	5

MEASUREMENT TECHNIQUES

In the following section, the employed measurement techniques are explained.

Optical OH* Measurements

Under atmospheric conditions, the electronically excited OH* radical emerges mainly in the reaction zone. Therefore, it is a well suited indicator for the heat release zone. If sampled and averaged over time, it can be used as an indicator of mean flame shape and an approximation of flame lift-off height. Its existence is very short and its decay can be described by the reactions (Dandy et al., 1992; Lee et al., 2003)

$$OH^* \leftrightarrow OH + radiation, \quad (2)$$

$$OH^* + M \leftrightarrow OH + M\ , \quad (3)$$

where Eq. (2) describes the radiation by transition to stable OH and M are molecular collision partners. A CCD LaVision camera was used (Imager Pro Plus 2M) with a resolution of 1600x1200 pixels and a LaVision IRO image intensifier. The OH*-signal was detected with a lens resolving wavelengths within 250 - 410 nm and multiple optical and transmission band-pass filters were applied to the camera system in order to block background noise and luminescence. The recorded and line-of-sight integrated volume and the measurement system positioning relative to the combustor are shown in Fig. 5. It is positioned in a way that two flames are sitting in a row with the line-of-sight direction.

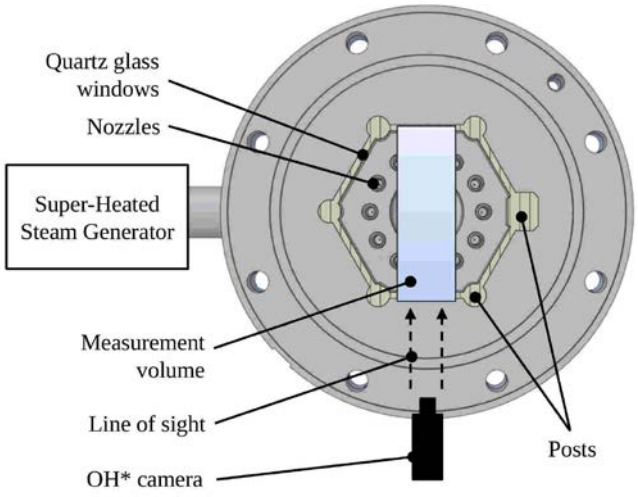

Figure 5 Top view onto the burner with cutting plane through the combustion chamber. Indicated OH* measurement volume and camera position.

Emissions Measurements

Exhaust gas is analysed after the converging section downstream of the combustion chamber with an ABB process gas analyser (Advanced Optima process gas analyser AO2000). The air cooled sampling probe is attached to a temperature controlled heated feed hose to the analyser in order to preserve the original chemical composition. The gas analyser is able to detect combustion products H_2O and CO_2, oxygen contents and pollutants. In the presented analysis, the focus for pollutant emission lies on carbon-monoxide (CO). Since the LHVs and subsequently the adiabatic flame temperatures are very low in all cases, NOx emissions are negligible. Since the emissions are constantly below or at the edge of the resolution capability of the analyser, they are not regarded further. CO emissions are shown on a dry basis and normalised to 15 % oxygen. Sampling of data is carried out with a frequency of 2 Hz over a range of 5 min. Achievable accuracies of the emissions measurement device are listed in (Hasemann et al., 2017).

EXPERIMENTAL RESULTS

In this section, the experimental results are presented in terms of CO emissions and averaged OH*-chemiluminescence profiles. First the results of the reference points for base load and part load are explained followed by the investigations on NG addition for part load stability improvement and lastly the simulated stack temperature increase for system efficiency improvement under base load conditions.

Base Load Reference Point

The first considered operating point is referred to as base load reference point later on. The base load point is located at 240 krpm full nominal load rotational speed of the turbine with a stack temperature of 1073 K. It is visualised in Fig. 3 in terms of overall electrical system efficiency over electrical system power output as well as in Fig. 4 as case #1b in terms of LHV.

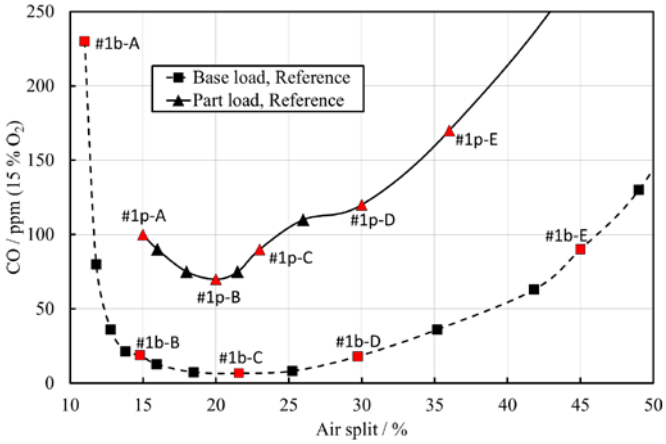

Figure 6 CO emissions over air split – base load and part load conditions – OH* figures from Fig. 7 and Fig. 8 highlighted red.

The dashed line in Fig. 6 depicts the resulting CO emissions over the air split representing the quantitative value for the air variation regarding the power plant system. The air split is defined as the air used in the combustor as primary air supply divided by the total compressor air supply. Since it is the critical design parameter for the combustion chamber to be set to a fixed value, all air variations are plotted over this value providing comparability. The nominal base load operation is characterised by a wide stable operational range with sufficiently low CO emissions from about 12.0 to 45.0 % of air split. The steep increase in CO emissions towards lean but near stoichiometric conditions (to the left side in Fig. 6) is characteristic and expected due to a shifted equilibrium state. Low jet velocities lead to low recirculation rates and hence bad mixing and presumably contribute to this behaviour. On the other hand the increase of the CO emissions to the fuel-lean side of the graph (to the right side in Fig. 6) is characterised by low adiabatic flame temperatures and hence slow reaction rates eventually obstructing a complete oxidation.

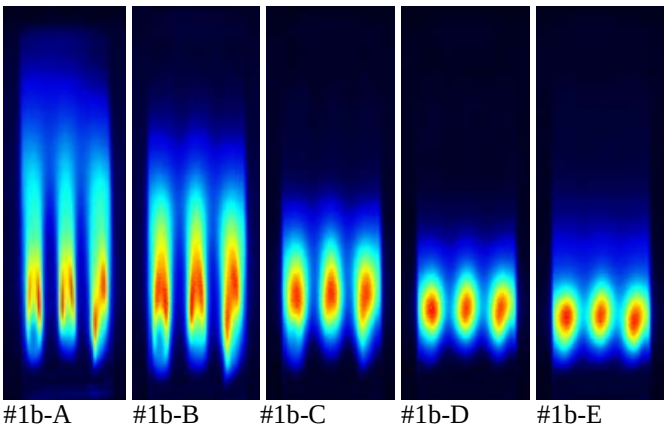

Figure 7 OH* figures – air split variation – base load.

In Fig. 7 an excerpt of the corresponding OH*-chemiluminescence figures is shown. The depicted operating points from the air split variation are highlighted red and labelled with the corresponding ID in Fig. 6 for better orientation. The appearance is changing from long discrete flames under near stoichiometric conditions (#1b-A) due to low jet velocities and hence bad mixing to more compact flames near the design point (#1b-C). Moving towards lean conditions the flame length decreases slightly further because of higher recirculation rates and better mixing. However the flame becomes unstable due to the low adiabatic flame temperatures in these conditions. It has to be pointed out that all presented OH* figures were normalised to its individual maximum values. Hence the intensities of the separate figures are not comparable to each other.

When highest achievable efficiencies are not the main goal, for example for heat up or comparable non stationary manoeuvres, this nominal base load operating point at a relatively low stack temperature level can provide a high level of operational stability.

Part Load Reference Point

The part load reference is defined at 180 krpm nominal part load rotational speed with a stack temperature of 1073 K. As illustrated in Fig. 4 as case #1p the heating value of the part load reference point of the hybrid power plant system is already much lower than in the base load case. This results in lower flame temperatures and overall less stable operating conditions for the combustor. Fig. 6 shows clearly that the CO emissions of the nominal part load operation are settling on a significantly higher level than in the base load case. The non-uniform shape of the curve is characterised by unstable operating conditions. These instabilities were supported by observed high fluctuations in emissions in all operating points.

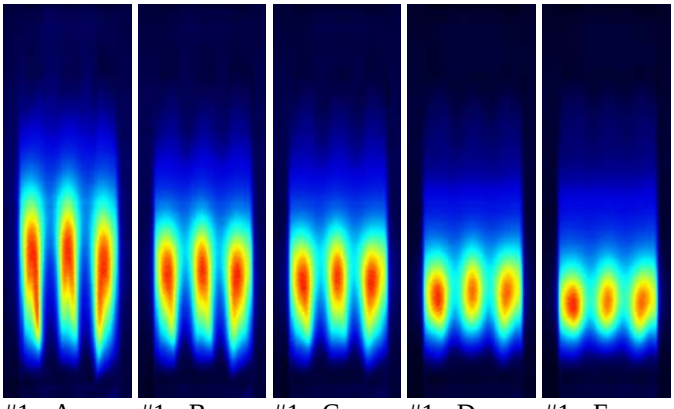

Figure 8 OH* figures – air split variation – part load.

In Fig. 8 the corresponding OH* figures to the operating points #1p-A to #1p-E are shown. The expected longer and more discrete flames towards stoichiometric conditions (#1p-A) are visible with a shift towards shorter and wider more volumetric flames at the lean end of the air split range (#1p-E). The change in appearance towards the fuel-lean conditions to a shorter flame is not as distinct as in the base load case which is based on the overall unstable conditions.

Since the CO emissions do not drop below 70 ppm even in the optimum operating point combined with the observed instabilities of the flame, finding a way for flame stabilisation is mandatory. As investigated in the next section a natural gas addition to the off-gas directly prior to the combustion chamber was chosen in order to increase the lower heating value and flame temperature.

Flame Stabilisation under Part Load Conditions via Natural Gas Addition

As pointed out in the previous section, the nominal part load operating point is not suitable for stable and clean operation of the power plant. A direct addition of natural gas prior to the combustion chamber to increase the heating value as well as the resulting flame temperatures was chosen as a possible solution. For this purpose, natural gas was added in discrete steps representing a power addition of 1, 2 and 5 kW to the combustion chamber.

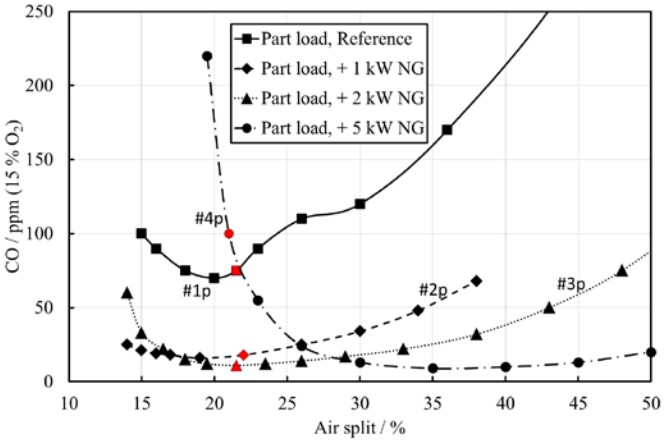

Figure 9 CO emissions over air split – part load conditions with NG addition – OH* figures from Fig. 10 highlighted red.

Fig. 9 shows with set #2p that an addition of only 1 kW already leads to a significant improvement of the CO emissions. Increasing the amount of added natural gas further to 2 kW (#3p) indeed results in a further reduced optimum of CO emissions, but simultaneously shifts the optimum operation air split to higher values.

This is an expected behaviour since the addition of fuel leads to more rich equivalence ratios with the same air split configuration pushing the optimum to higher air split values. This gets even more obvious in case #4p which changes the equivalence ratio remarkably and pushes the optimal operating point far out of the targeted suitable range for the power plant system.

Since the addition of natural gas at a near constant air split (as marked red in Fig. 9) shifts the equivalence ratio closer to stoichiometric conditions (from #1p towards #4p), a slight elongation of the flame is visible in Fig. 10. A significant change in flame shape or appearance

corresponding to the remarkable drop in CO emissions is not noticeable.

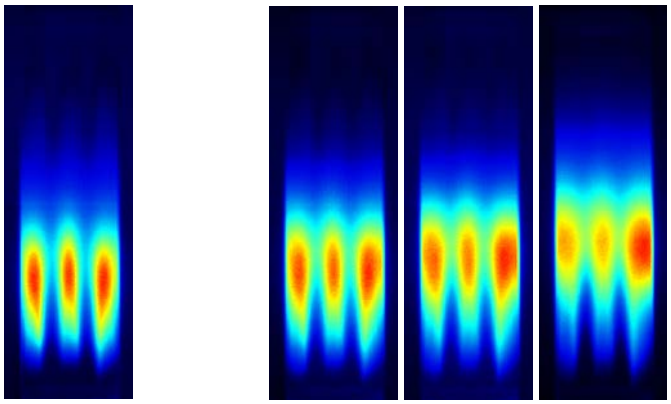

Figure 10 OH* figures – part load conditions with NG addition.

Apparently the addition of natural gas to the off-gas prior to the combustion chamber can be a credible solution to stabilise unstable operating points like the reference part load point presented. An addition of a relatively small amount of extra fuel can lead to a remarkable drop in CO emissions for operating points around the operational limit. Since a significant change in the resulting equivalence ratio is not manageable with a fixed air split setup, this possibility cannot be used for operating points located far beyond the original operating limit, but to extend the operational range by a significant amount.

Increase of Stack Temperature and System Efficiency under Base Load Conditions

The good CO emissions values and flame stability in the base load reference point with a moderate stack temperature of 1073 K suggest utilising the available margin for an improvement of the achievable system efficiency. As explained before an increase of the stack temperature of the SOFC system will lead to a higher overall system efficiency as well as decreased heating values in the resulting off-gas, hence more difficult operating conditions for the combustion chamber. The goal for the following investigations is to approach the possible manageable stack temperature levels to define an efficient operational strategy for the power plant in the future.

Since the first simulated increases of the stack temperature to 1083, 1093 and 1103 K did not lead to any significant change in CO emissions around the design point of the system in terms of air split, no complete air split variations are carried out for these temperatures as can be seen in Fig. 11. For 1013 K stack temperature however a noticeable rise in CO emissions is observed being the reason

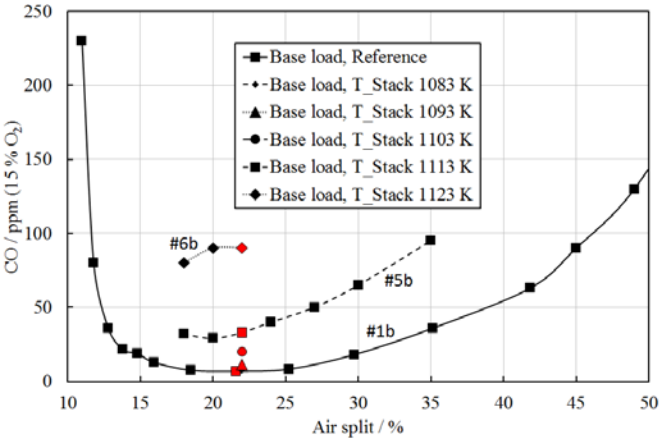

Figure 11 CO emissions over air split – base load conditions with stack temperature increase – OH* figures from Fig. 12 highlighted red.

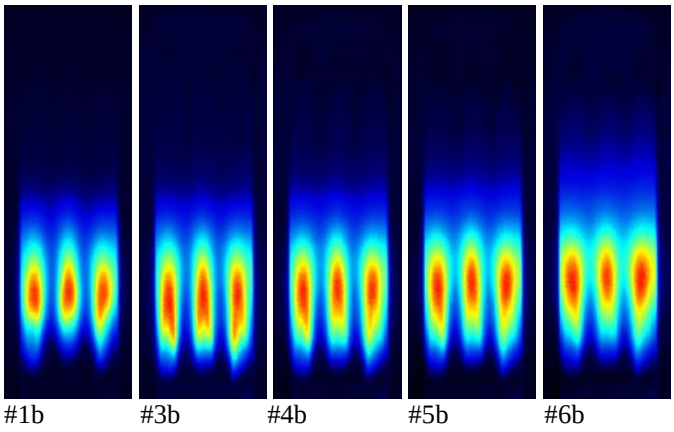

Figure 12 OH* figures – base load conditions with stack temperature increase.

to perform a complete air split variation at this temperature level. Since the best achievable CO emissions level for this case is around 30 ppm, the boundary for a reasonable steady operation of the system seems to be reached here.

As a further increase to the maximum allowable stack temperature of 1123 K shows a significant increase in emissions and instabilities of the flame were observed, no complete variation was carried out for this case either.

A correlation between the rising CO emissions and observed instabilities and the appearance in terms of OH*-chemiluminescence in Fig. 12 could not be observed. An explanation could possibly be the combination of the counteracting effects of leaner conditions and lower flow speeds and hence recirculation rate towards #6b leading to the observable similar appearance.

CONCLUSIONS AND OUTLOOK

The carried out investigations of the SOFC off-gas combustor demonstrated that an operation at the defined base load operating point with changed operating conditions due to an adjusted system setup is possible, stable and characterised by low CO emissions.

For the part load case, the experiments revealed instabilities and unsuitable high emissions which can be traced back to the significantly decreased LHV of the off-gas

compared to the case investigated in previous work (Bücheler et al., 2017). It was found that an addition of natural gas to the off-gas prior to the combustion chamber leads to a sufficient increase of the LHV and flame temperatures to stabilise the combustion and reduce the emissions significantly. This inevitably leads to a reduction in the achievable system efficiency but assures the successful operation in affected operating points with the available combustor for the initial system setup.

For the base load operation a possible enhancement of the system efficiency was distinguished via increase of the fuel cell stack temperature. The limits of this improvement due to degrading operating conditions for the combustion chamber were approached and quantified.

It is planned to expand the investigations to additional operating levels in terms of system power output. Namely intermediate points between the considered part load and base load references as well as even lower system power levels to approach the limits of the system for the combustion chamber. Furthermore the operation with biogas driven SOFC off-gas leading to even lower heating values is planned to be investigated.

NOMENCLATURE

DLR	German Aerospace Center	-
FLOX®	Flameless Oxidation	-
LHV	Lower Heating Value	-
MGT	Micro Gas Turbine	-
MILD	Moderate or Intense Low-oxygen Dilution Combustion	-
NG	Natural Gas	-
SOFC	Solid Oxide Fuel Cell	-

ACKNOWLEDGMENTS

This research was supported by the European Union's Horizon 2020 "Bio-HyPP" project. Additionally we would like to thank Hannah Bower for the assistance with the OH*-chemiluminescence setup.

REFERENCES

[1] Hohloch M., Huber A., and Aigner M. (2017). Analysis of Operational Strategies of a SOFC/MGT Hybrid Power Plant. In: Proceedings of the ASME Turbo Expo 2017 – GT2017-65013.

[2] Bücheler S., Huber A., and Aigner M. (2017). Development of a Jet-Stabilized Combustion System for the use of Low-Caloric SOFC Off-Gas. In: Proceedings of the ASME Turbo Expo 2017 – GT2017-64447.

[3] Hermann F., Palsson J., and Mauss F. (2002). Combustor Design Analysis for SOFC Off-gases. In: 5th Solid Oxide Fuel Cell Forum, Lucerne, Switzerland.

[4] Loukou A., Voss S., Mendes M., Raimondi A., and Trimis D. (2009). Parametric experimental investigation of a small scale packed bed reactor for Thermal Partial Oxidation. In: 4th European Combustion Meeting, Vienna, Austria.

[5] Voss S., Mendes M., Pereira J., and Trimis D. (2009). Comparison of Experimental and Numerical Results of Ultra-Lean H2/CO Combustion within Inert Porous Media. In: 4th European Combustion Meeting, Vienna, Austria.

[6] Wünning J., and Wünning J. (1997). Flameless oxidation to reduce thermal NO-formation, Progress in Energy and Combustion Science. 23(1), 81-94. DOI: 10.1016/S0360-1285(97)00006-3.

[7] Cavaliere A., and Joannon M. (2004). Mild Combustion. Progress in Energy and Combustion Science. 30(4), 329-366. DOI: 10.1016/j.pecs.2004.02.003.

[8] Flamme M. (2001). Low NOx Combustion Technologies for High Temperature Applications. Energy conversion management. 42, 1919-1935. DOI: 10.1016/S0196-8904(01)00051-6.

[9] Lückerath R., Meier W., and Aigner M. (2008). FLOX® Combustion at High Pressure With Different Fuel Compositions. Journal of Engineering for Gas Turbines and Power. 130(1), 011505. DOI: 10.1115/1.2749280.

[10] Flamme M. (2004). New combustion systems for gas turbines (NGT). Applied Thermal Engineering. 24, 1551-1559. DOI: 10.1016/j.applthermaleng.2003.10.024.

[11] Lammel O., Stöhr M., Kutne P., Dem C., Meier W., and Aigner M. (2011). Experimental Analysis of Confined Jet Flames by Laser Measurement Techniques. In: Proceedings of the ASME Turbo Expo 2011 – GT2011-45111.

[12] Rödiger T., Lammel O., Aigner M., Beck C., and Krebs W. (2013). Part-Load Operation of a Piloted FLOX® Combustion System. Journal of Engineering for Gas Turbines and Power. 135(3), 031503-01. DOI: 10.1115/1.4007754.

[13] Zanger J., Monz T., and Aigner M. (2013). Experimental Investigation of the Influence of Combustor Cooling on the Characteristics of a FLOX®-Based Micro Gas Turbine Combustor. Progress in Gas Turbine Performance. 165-184. DOI: 10.5772/54405.

[14] Monz T., Stöhr M., O'Loughlin W., Zanger J., Hohloch M., and Aigner M. (2015). Experimental characterization of a swirl stabilized MGT combustor. In: Proceedings of the ASME Turbo Expo 2015 – GT2015-42387.

[15] Dandy D., and Vosen S. (1992). Numerical and Experimental Studies of Hydroxyl Radical Chemiluminescence in Methane-Air Flames. Combustion Science and Technology. 19, 131-150. DOI: 10.1080/00102209208951816.

[16] Lee J., and Santavicca D. (2003). Experimental Diagnostics for the Study of Combustion Instabilities in Lean Premixed Combustor. Journal of Propulsion and Power. 19, 735-750. DOI: 10.2514/2.6191.

[17] Hasemann S., Huber A., Naumann C., and Aigner M. (2017). Investigation of a FLOX® based Combustor for a Micro Gas Turbine with Exhaust Gas Recirculation. In: Proceedings of the ASME Turbo Expo 2017 – GT2017-64396.